25 November 1977, Volume 198, Number 4319 **SCIENCE**

Spark Discharge: Application to Multielement Spectrochemical Analysis

John P. Walters

Summary. Spark discharge is shown to be a cyclic process of energy dissipation, with one spark in a time-connected train influenced by its relation to predecessor sparks. Spectroscopic instruments having temporal, spatial, and spectral resolution indicate that the light emission is highly ordered with cylindrical symmetry about the current-conducting spark channel. The favored spatial coincidence is between the channel and the most highly ionized and most excited species sampled from the cathode, with less ionized and less excited species emitting farther outward. Light absorption occurs to such an extent that there are full line reversals in excited states of magnesium ions, distant from the channel. Schlieren data indicate a toroidal structure in the postdischarge environment. Charge transfer, Penning ionization, and sensitized fluorescence are thought to be the chemical mechanisms responsible for the spectroscopic topography. Experiments in spectrochemical analysis based on the topography and designed for increased sensitivity, reduced matrix effects, and simpler spectra are discussed.

The sudden discharge of energy stored at high voltage in a capacitor is commonly called a spark discharge. If one observes such a discharge across a pair of separated electrodes, the phenomenon appears to consist of a single, somewhat irregular event. But such is not the case. Rather, an orderly collection of many interacting events comprises the discharge. The events may be controlled in many ways. Taken collectively, they constitute a process of energy dissipation which may be called spark discharge. One by-product of spark discharge is emitted light.

Spark discharge is intrinsically interesting as a process. It also has demonstrated practical utility, in that the intensity and wavelength distributions of the light emitted during spark discharge are related to the elemental composition of the spark-gap electrodes. Analytical spectrochemical spark discharge procedures can be used in the quantitative determination of most elements present in solid, alloyed electrodes. The method has widespread applicability as a routine tool for the industrial quality control of metals and alloys. It is particularly rapid; up to 30 elements can be determined simultaneously in less than 60 seconds on an electrode prepared for analysis simply by belt-sanding.

Even though this analytical method is in widespread use and is economically competitive with other approaches, its performance is still in need of improvement. The sensitivity needs to be increased by about 100-fold from the current levels of a few parts per million; this improvement would make possible analysis of, for example, minute but purposeful trace additions to an alloy during its molten refining introduced in an effort to adjust grain growth and nucleation during its solidification. In addition, the precision must be improved by about tenfold from its present ± ½ percent of the amount present to allow, for example, analysis of relatively expensive major alloying elements (Ni or W). This advance could provide improved control of melt compositions during alloy refinement at optimum economy, and with closer conformity to chemical specifications.

With improved performance in spectrochemical analysis, better and expanded uses of the chemical data should follow. It is reasonable to expect more use of compositional data in the economic management of raw materials, in organizing factory operations to give optimum use of furnace energy, and, with other controls, to predict the final mechanical properties of an alloy at the pouring stage rather than after it has been made and can no longer be changed. Although these are real and important reasons to try to improve spectrochemical performance, the key to such progress is not instrumental but rather chemical. With spark sampling and excitation, the questions that need answers are not how to make a more precise spark source, but rather, how light is generated during spark discharge, and, if the responsible phenomena are understandable, how they can then be more precisely controlled at the atomic level. Observation, sorting, and control of the physical and chemical events comprising the process of spark discharge, for the express purpose of improved spectrochemical analysis, form the basis of the information I report here.

The Spark Discharge Process

Spark discharge is composed of a surprisingly large number of component events. For clarity, they are grouped in Fig. 1 into categories numbered in order of the time sequence in which the events occur during discharge. Perhaps more

---

The author is professor of chemistry at the University of Wisconsin, Madison 53706.

important than the number of events is the fact that their interaction is cyclic. The properties of one spark may strongly (or weakly) determine the properties of the next, and that of the next, and so on. It thus is difficult to describe the properties of one spark as typical or fundamental. I describe instead one or another member in a time-connected sequence of individual discharges (called a spark train). The chemical aspects, or appearance, of any selected member may be very much influenced by its time relation to its predecessors.

The events composing spark discharge fall into three classes. The first includes those that allow current to pass between the electrodes. These events consist of the formation of an electrically conductive path or bridge between the electrodes (block 1), connection of the ends of the path to specific points on the electrode surfaces (block 2), and then conduction of current at low resistance along the path (block 6). At atmospheric pressure, the path is visibly well defined and is termed a channel for current conduction. The balance of electrical charge (positive and negative) is kept equal along most of its length, until the electrode surfaces are approached. Space charge imbalances then arise, with the negative cathode showing a higher surface environment of positive ions than the anode. It is customary to consider the events in this first class as constituting "a spark." However, such a spark would do little practical work, and other classes of events must also be considered.

The second class includes those events that cause light that can be used for analysis to be emitted from the space between the electrodes. These consist of the conversion of a portion of the solid electrode surface to a vapor (block 3), movement of the vapor away from the immediate electrode surface into the region between the electrodes (block 5), and chemical reaction of the vapor with other reagents (block 7) to cause it to emit a discrete line spectrum (block 9). This class of events is of consequence for analysis but of presently unknown importance in determining the electrical properties of spark discharge. This importance will depend upon the chemistry that is occurring in the third class of events, all those events that determine the environment remaining between the electrodes after current conduction ceases (block 11).

The time between individual discharges in a spark train, or the repetition rate, is usually controlled by the hardware (*1*). So is the amplitude of the current conducted by the spark channel as a function of time (*2*). At atmospheric pressure, the diameter of the spark channel increases with increasing current (current is conducted at approximately constant density in the channel). The types of products and their concentrations in the postdischarge environment are determined, at least in part, by the overlap in spatial volume between the spark channel and moving electrode vapor. Moreover, if the products are still present when the next spark in the train is caused, they will influence the direction taken by the channel between the electrodes for the next spark. This interaction will determine what new vapor-channel processes will occur, and a cycle will be established between the events in blocks 11 and 1, linked by the hardware in block 12. It follows that the degree of interaction of the events in the central blocks of Fig. 1 will determine in part how the chemistry of sparks in a time-connected train influences the light emitted for chemical analysis.

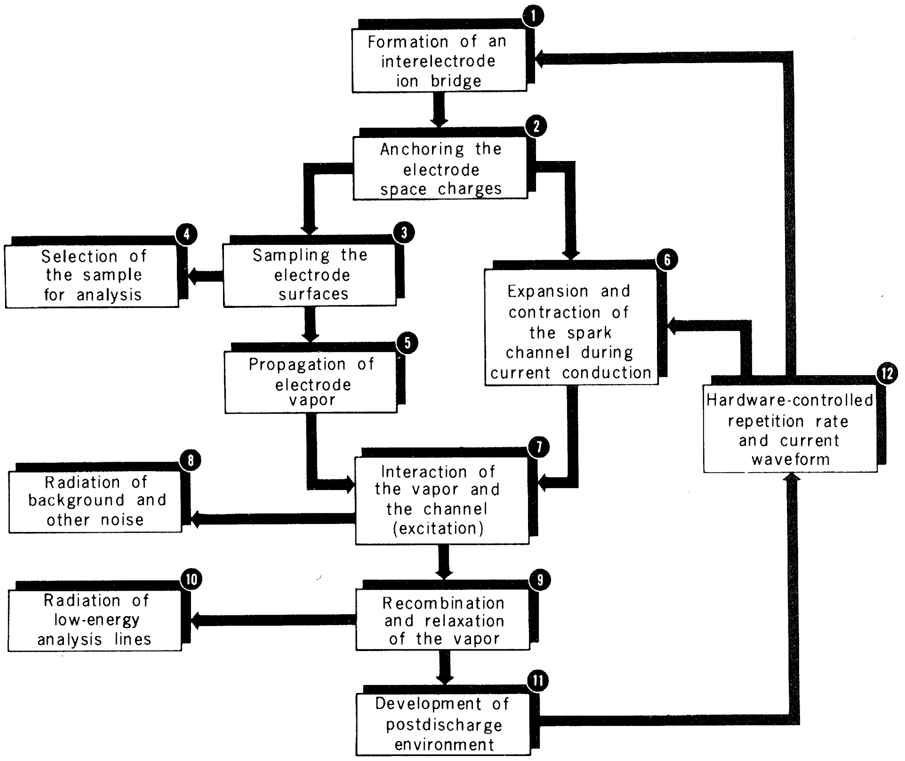

Fig. 1. Block diagram of the process of spark discharge.

Two important criteria for chemical analysis of the electrodes are the accuracy and sensitivity of the method. Because of the large number of events comprising spark discharge, it is necessary to prepare calibration graphs relating the concentrations of the impurities or alloying components in the electrodes to the light intensity in a particular spectral line. The method of analysis is based on a comparison of line intensities from unknown samples with these calibration graphs (*3*). In order for this approach to succeed, the intensity-concentration relation must remain stable over the time between calibration and analysis. In view of the complex chemistry of spark discharge, such stability is not readily achieved. Thus, the accuracy of the analysis may be directly traced to the precision (repeatability) of the many events shown in Fig. 1.

The accuracy is also affected by the relation between the portion of the sample that was converted to vapor and excited to emit light and the whole-sample composition. The attack of the electrode by the spark is superficial, and then only of consequence for the cathode (*4*). The sample actually selected for analysis (block 4) is determined in part by the location of the cathode space charge (called the cathode "spot") on the electrode surface (block 3). Ironically, the accuracy of an entire analysis may be determined by a factor so seemingly insignificant as a draft in the chamber holding the electrodes. Such a draft may cause a series of sparks to wander to a spot on the cathode surface that is locally heterogeneous in a particular alloying element.

The sensitivity is also related to the repeatability of the events in Fig. 1. Usually, the lowest concentration of an element that can be reliably determined by this method (called the "limit of detection") is not set by the total amount of light emitted in the spectrum of that element. Instead, it results from the inability to distinguish changes in the continuous noise (or spectral background) from changes in the line intensity due to concentration changes in the electrode. This difficulty is compounded by the chemistry of spark discharge. The background noise originates largely from the interaction of the sampled electrode vapor with the spark channel as the vapor moves into the spark gap at high velocity (block 8). However, the radiation commonly used for analysis occurs after this interaction, as the ions in the moving electrode vapor recombine with free electrons and relax back to low-energy excited electronic configurations (blocks 9 and 10). In some cases, the spectral lines are even detected in different spatial regions from those emitting the background noise. Because two completely different sets of chemical conditions and reactions control these two signals, fluctuations in one may show only marginal correlation to fluctuations in the other (*5*). Unless one can minimize these fluctuations by making the chemistry causing the signals precisely repeatable, the sensitivity will be reduced.

My students and I have observed much, if not most, of the chemistry presented in Fig. 1 [see also (*6*) for a partial review of the work of others]. I would emphasize that any chemical event may be influential to varying degrees for different elements in a host (matrix) electrode. Thus a large number and variety of analyzed comparison standards must be available for calibration in analysis. Often, the composition of the standards must be very close to that of the unknowns, which is an inconvenience for those who make the standards as well as for those who use them. Clearly, experimental control of the chemistry of spark discharge would be beneficial even if it did little more than improve the accuracy and sensitivity of the analysis carried out, and at the same time reduce the number of calibration standards required (*7*).

I will describe more specifically those chemical aspects of spark discharge we either have controlled in our work or feel now need to be controlled since they influence the radiation used in multielement spectrochemical analysis. In this description, I will focus on blocks 1, 5, 7, 9, and 11 (Fig. 1), since our knowledge of the events comprising them is most defined.

Experimental Tools

To observe and identify specific chemical events active in spark discharge, we found it necessary to build instrumentation for the spatial, temporal, and spectral examination of the light emitted, absorbed, or refracted in the region between the electrodes (*8*). At the same time, we devised means for causing all discharges in a train to follow a predicted and repeatable path between the electrodes. Precisely triggerable spark sources that did not electrically interfere with sensitive measurement and control electronics were also built.

To optically obtain spatial resolution in the spark gap at the submillimeter level, pairs of parabolic mirrors were arranged to cancel image aberrations (*9*). A spatial resolution of 0.03 millimeter at a magnification of unity was obtained. With one of the mirrors rotating at 3600 revolutions per minute, we achieved a time resolution of or exceeding 0.1 microsecond (*10*). A variety of grating spectrometers (typical resolution, 0.1 angstrom) were incorporated into the optical systems. In one case, the imaging and time-resolving optics were made an internal part of the spectrometer (*11*). Resolutions of this order are necessary to separate interacting events during spark discharge, since a typical electrode separation is only 2 to 3 mm and complex emission spectra may change rapidly as little as 0.1 to 0.3 mm away from the cathode surface (*12*).

We achieved full experimental control over the time separation between individual discharges in a train by using a digital computer to trigger a hydrogen-thyratron switch in one type of spark source (*13*). In another type that used a quarter-wavelength transmission line for high-voltage production (*14, 15*), precision pulse-generators sufficed. We adjusted the spark current by shunting the spark gap with a high-voltage diode (*16*) and splitting the current between the spark and diode paths with a variable inductor (*17*). With careful component layout [see, for example, (*1, 13*)] in these sources (and with the use of simple electrical wiring) we were able to remove the last annoying traces of electrical interference with the adjacent control electronics.

By following a guideline of Thackeray (*18*), we were able to locate and stabilize the spark paths. A gas flow-jet surrounding a W pin anode (*19*) directed a circular stream of Ar between the electrodes. This stream defined the spark channel location through preferential ionization in the Ar path resulting from collisions of electrons with high-energy, metastable Ar $^3P_0$, $^3P_2$ states (*20, 21*). We were able to confine the movement of the cathode spot to 0.2-mm tolerances by preventing any changes in current direction during each discharge (*22*). Slow rotation of carefully machined cathodes, absorption of sharp sound waves, and prevention of massive electrode erosion from high spark currents also were required. By carrying out all the steps described above, we were able to keep spark locations stable at submillimeter tolerances for up to 2 hours of continuous operation at up to 10,000 sparks per second.

One can develop a feeling for the stability appropriate for the fundamental observation of spark discharges from an examination of Fig. 2. One oscillatory discharge with four full current reversals in still N_2 is shown in Fig. 2B. Seventy controlled discharges with unidirectional, transient-free current in flowing Ar are shown in Fig. 2A.

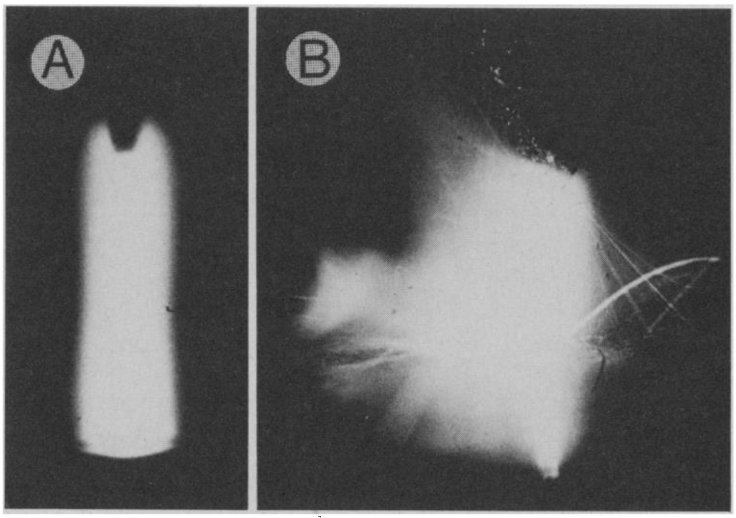

Fig. 2. Stable (A) and unstable (B) spark discharge.

Light Emission

Once a train of discharges has been positionally stabilized, the light emitted from any one of the discharges reveals striking order and regularity (*23*). Most of the emission resides in line spectra radiated from ions of the vapor (charged + and 2+) sampled from the cathode. The order (or topography) unfolds in time and space as the vapor moves vertically away from the electrode surface and radially outward from the spark channel.

The most pronounced character of the emission topography is the spatial (and temporal) separation of light between ionized and un-ionized species in the vapor. Figure 3 shows a partial sample of the spatial-temporal emission topography of a selected set of spectral lines photographed by Goldstein (*24*). The emission was detected in an isolated cylindrical region with a height of 0.05 mm and a maximum diameter of 5 mm, located 0.05 mm away from a Cu cathode. The term "radial displacement" means distance outward, along a radius, from the straight spark channel that is conducting current between the vertical, spark-gap electrodes (*25*). "Line density" is a logarithmic measure of the amount of blackening on the photographic plate used to record the spectral line emissions at the designated times after the start of the spark discharge current. It is approximately proportional to the amount of light emitted in the designated spectral line.

At any one time (viewing down a vertical column in Fig. 3), the light from more energetic or more highly ionized vapor species is structured in an oxbow or dumbbell shape near the center of the spark channel. The peak in the radiation from Cu^{2+} (Cu III line, trace C) is closer to the channel center than that from Cu^+ (Cu II lines, traces D and E). That from Cu^+ is closer to the channel center than that from un-ionized Cu atoms (Cu I lines, traces F, G, and H). The more energy stored in a particular vapor species, the more light detected in regions close to the channel compared to away from it (compare trace D with trace E, trace F with trace G). The pattern is maintained and becomes more pronounced as time elapses (compare the columns from left to right in Fig. 3).

I interpret the patterns in Fig. 3 to be the effects of chemical reactions between the moving electrode vapor and the current-conducting spark channel. The reactions appear to begin for high-current sparks (> 50 peak amperes) within 0.1 mm displacement from the cathode surface. Here the first light detected (< 0.1 microsecond from the first current) in visible and ultraviolet wavelengths (8000 to 2000 Å) is in the ionic spectrum of the electrode material. Thus Al first radiates Al^+ lines, Cu Cu^+ lines, and Zn Zn^+ lines.

As the electrode vapor moves away from the cathode surface (< 0.3 mm displacement), light is emitted in the more ionic spectra, for example, Al^{2+}, and from more energetic states of a particular ion (*26*). The trend, although occurring

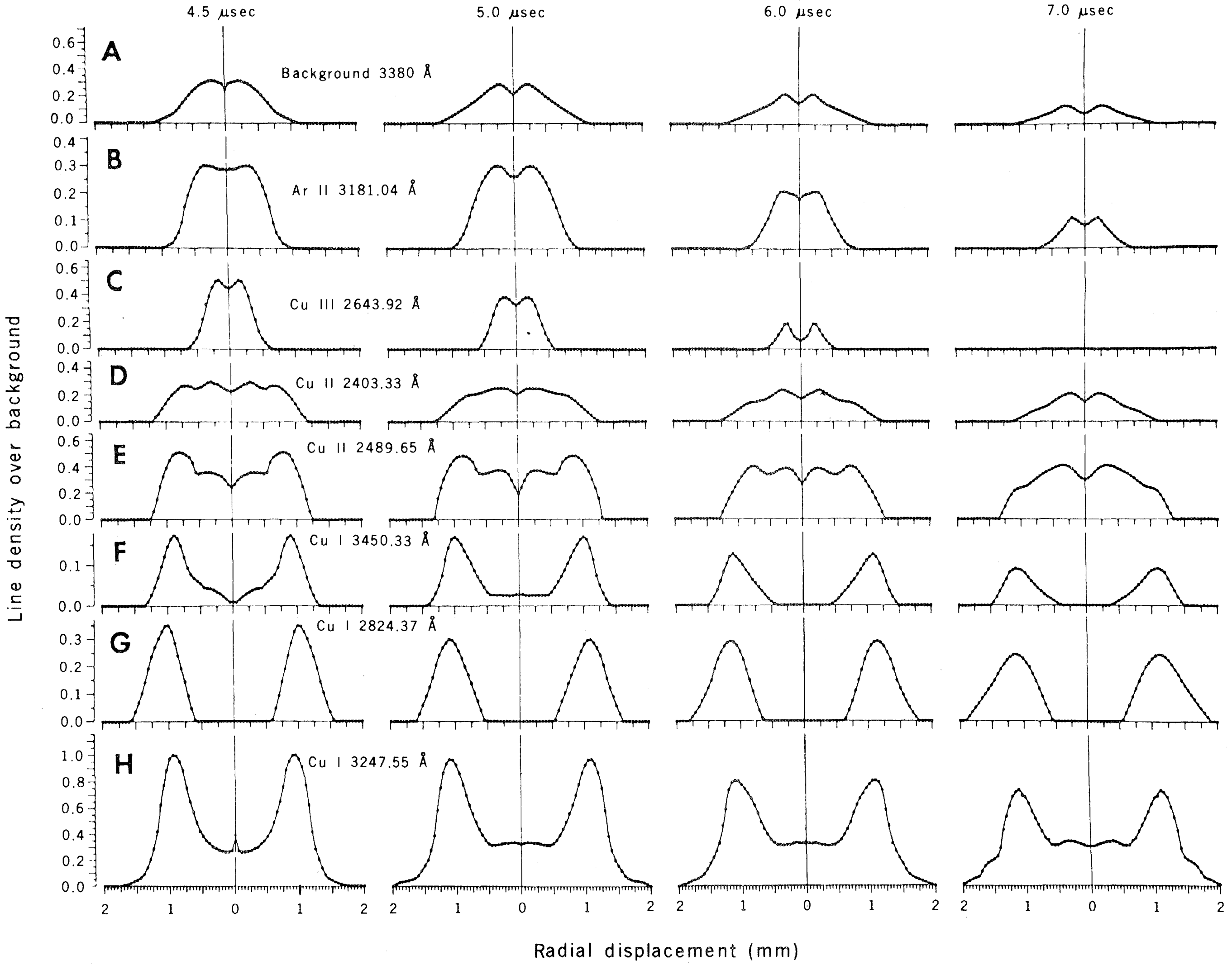

Fig. 3. Spatial and temporal topography of spark emission from selected spectral lines of Cu and Ar detected 0.05 mm from a Cu cathode.

rapidly and over small distances, is quite regular. Upon complete traversal of the cathode space charge, the electrode vapor is emitting line spectra from high-energy states in multiply charged ions. The vapor appears to originate from a small electrode area (< 0.2 mm in diameter) directly beneath the cathode space charge. When clear of the ion-rich space charge, the vapor cloud has not expanded in volume significantly. Thus, the emission from the most energetic, most highly ionized species of the vapor starts in direct spatial coincidence with the spark channel.

As the vapor moves farther away from the cathode, its volume (as detected by its emission) appears to increase. I interpret this as primarily a thermal effect (*27*), although contributions from the magnetic field surrounding the spark channel are not discounted. This expansion removes progressively larger fractions of the moving vapor from immediate contact with ions of the current-conducting channel (principally Ar^+ and Ar^{2+}). Reactions influencing almost all of the vapor when in the space charge then act upon a smaller relative proportion of it. Relaxation from high to low electronic energy occurs, with radiation following an orderly, cascading type of pattern between progressively lower energy, less excited electronic states. Since the vapor continues to move during the time required for a sufficient number of ions to emit a detectable spectrum, the spectral lines appear with the spatially distinct topography shown in Fig. 3.

Eventually, some unknown fraction of the relaxed vapor ions recombines with an electron. It would appear that the reactions are of the form (*28*):

$$Al^{2+} + e^- + e^- \rightleftarrows (Al^+)^* + e^-$$
$$Cu^{2+} + e^- + e^- \rightleftarrows (Cu^+)^* + e^-$$

with the products first forming in only a few highly excited electronic states. These excited products then relax in a cascading manner, such that the light they emit while so doing is arrayed in spatially distinct rings or shells about the spark channel.

The portion of vapor remaining in physical contact with the spark channel appears to be progressively reexcited as it moves farther from the cathode. Goldstein detected little, if any, line emission from the channel regions before the electrode vapor passed the region of observation (*24*). Then, a moving front of light composed of both channel and vapor spectra was detected. Spatial, temporal, and spectral analysis suggests that this light originates from the exchange of charge and potential (electronic) energy between channel ions (for example, Ar^+ and Ar^{2+}) and moving vapor ionized earlier while passing through the cathode space charge. Reactions of the type

$$Cu^+ + Ar^{2+} \rightleftarrows Cu^{2+} + Ar^+$$

and

$$Cu^+ + (Ar^+)^* \rightleftarrows (Cu^+)^* + Ar^+$$

are examples we have investigated (*29*).

Unfortunately, the exact reaction paths are still elusive. The puzzle remains to be unraveled, in part because of the large number of possible combinations of excited reactants and products that are expected on the simple grounds of conservation of total energy (kinetic and potential) in the reaction. In computer simulations, several thousand likely combinations were revealed for just the reaction of Cu^+ with $(Ar^+)^*$. The problem is complicated by the difficulty of isolating emission from a set of reactants before (or just as) they first react.

Similarly, the cathode space charge is so small, and reactions therein occur so rapidly, that it is difficult to determine what is happening. A few analyses that I carried out [see, for example, (*26*)] indicated that the exchange of energy between space-charge ions and freshly sampled electrode vapor could occur through reactions similar to those in the spark channel, for example, reactions of the form

$$Ar^+ + Cu \rightleftarrows (Cu^+)^* + Ar$$

or

$$Ar^{2+} + Cu^+ \rightleftarrows (Cu^{2+})^* + Ar^+$$

or

$$Ar^+ + (Cu^+)^* \rightleftarrows (Cu^{2+})^* + Ar$$

The last type of reaction is particularly interesting and appears to occur to some degree for Al electrodes. It could account for the high ionization and excitation exhibited by electrode vapor in traversing the space charge.

Although the total amount of energy transferred to most of the electrode vapor in traversing the full space charge is relatively large (~ 80 to 100 electron volts), I suspect that this energy transfer is accomplished by the progressive accumulation and storage of smaller amounts (~ 5 to 10 ev). Such processes are known from other experiments (*30*) and have been termed stepwise or staircase excitation (or ionization).

Staircase ionization does not require the sudden transfer of large amounts of either kinetic or potential energy between space-charge ions and moving electrode vapor species. Instead, what is required is a large number of sequential, rapid, low-energy exchanges with the products of one exchange serving as the reactants for the next. To be a consequential ionization mechanism, the intermediate (excited) energy states of product atoms (or ions) would have to store the reaction energy for enough time to serve as stable reactants for the next encounters. Although the times between collisions in the cathode space charge are not known, my experiments with Al and Cu electrodes indicate that staircase ionization is an important factor (*26*). The process is compatible with the low-potential drops (< 100 volts) Coleman and I have measured across the electrodes of a spark gap (2 to 7 mm) in Ar (*31*).

Light Absorption

We detected the topographical information in Fig. 3 by viewing the discharges from a "side-on" direction, that is, at right angles to the vertically oriented spark channel. The emitted light had to pass through the outer regions of the cylindrical discharge volume before detection. It is to be expected that some absorption of some line emissions would occur as a consequence, perhaps establishing the basic spatial profile or shape of some of the emission lines.

Scheeline and Walters have investigated by computation (*32*) some basic effects of light absorption by species in the outer zones (radial wings) of the spark volume. From these studies, we were somewhat surprised to learn just how severely relatively small amounts of predicted absorption could distort the spatial profile of an emission line.

It is predictable that absorption would simply reduce the amount of light detected. However, it is the arrangement of the absorbers in a cylindrical ring around the (inside) emitters that causes the absorption to alter the detected spatial shape of the emitted light. When viewed from the side, more absorbers lie away from the spark channel than in line with it. The oxbow emission shape of a line (for example, Fig. 3, trace H) is detected as more centered and less peaked (for example, Fig. 3, trace C) when absorption occurs than when there is no absorption.

Since much insight into the chemical aspects of spark discharge can be obtained from the relative spatial shapes of emission lines, any events that can change their shapes are of interest. An example is the rather abrupt cessation of detectable emission from low-energy lines of the electrode vapor. Goldstein (*24*) has photographed this process for Cu, Ag, and Au. It occurs at distances of 1 to 2 mm away (radially) from the center of the spark channel (see Fig. 4 for vapor sampled from a Cu cathode).

It is logical that an outer, cylindrical shell of absorbers would confine the low-energy emission to spatial regions coaxially arrayed along the spark channel. The expected absorbing species would be simply nonexcited, nonradiating forms of the emitters. When a Cu cathode was sparked, neutral Cu atoms were first suspected (neutral Au atoms would be suspected for a Au cathode). Goldstein's spectroscopic searches for Cu absorbers produced initial negative results. Rentner *et al.* (*33*) recently detected partial absorption from neutral Cu atoms.

However, large amounts of absorption were detected in Mg by Coleman and Walters (*34*) and Klueppel and Walters (*35*). The absorption was so severe that transmission of light from the channel through the outer wings for a few lines was completely blocked, producing a phenomenon known as spectral line self-reversal. The most surprising aspect of this phenomenon was not the reversal (*36*), but rather that it occurred from ionized and excited absorbers that apparently were located in the outer wing regions of the spark gap.

Figure 5 shows a partial segment of a spatially and temporally resolved spectrum (photographed by Klueppel) in which these reversals appear. The radial displacement is measured outward, symmetrically from the center of the spark channel (marked "zero"). Spectral line self-reversal is first detectable in the lowest energy electronic state of Mg^+ (the $^2S_{1/2}$ ground state) starting at the point where the oxbow-shaped emission is a maximum, at about 0.5 mm away from the spark channel center (lines A and B). Reversal in the lines of the first excited state is first detected, surprisingly, farther outward, where intuitive expectations would suggest a cooler environment containing less, not more, excited species (lines C and D).

The spectroscopic picture must, however, be interpreted carefully, since it differs from what a thermal equilibrium model would suggest (*37*). Consideration must be given to the manner in which the spectra were photographed (*38*). For example, the detected spatial separation of the reversals in excited and ground state ion lines may arise from physical (spatial) separation of the absorbing species, or it may result from differences in the number of excited states and their relative absorptivities in a common spatial region. In order to sensibly differentiate between these possibilities, one would need a knowledge of the spatial distribution of possible chemical reactants that could produce excited states in cool discharge regions, as well as computer simulations (*39*) that predict how absorption and emission would appear in our experimental arrangement. We have carried out studies with refracted light as part of this investigation, the first results of which follow.

Light Refraction

The absorption data in Fig. 5 must be analyzed in terms of the number of potential absorbers left in the space between the electrodes from earlier discharges, as well as after current ceases in an isolated, emitting spark. The spatial distribution of such postdischarge products may be detected in refraction experiments after a train of discharges has been positionally stabilized.

Hosch (*40*), Klueppel *et al.* (*41*), and Rentner and Walters (*42*) have observed structure, order, and regularity in the postdischarge environment between re-

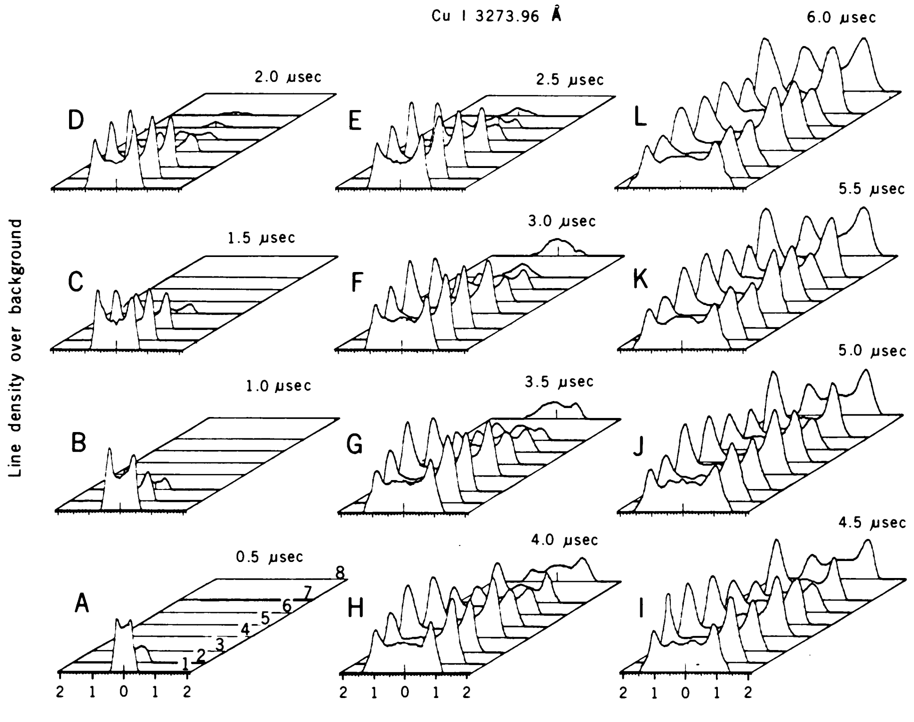

Fig. 4. Spatial and temporal topography of spark emission from the Cu neutral-atom line at 3274.0 Å at selected distances from a Cu cathode electrode; the distances [shown in (A)] are: 1, cathode surface; 2, surface + 0.20 mm; 3, surface + 0.40 mm; 4, surface + 0.75 mm; 5, surface + 1.00 mm; 6, surface + 1.25 mm; 7, surface + 1.50 mm; and 8, surface + 1.95 mm; anode-cathode separation, 2.00 mm.

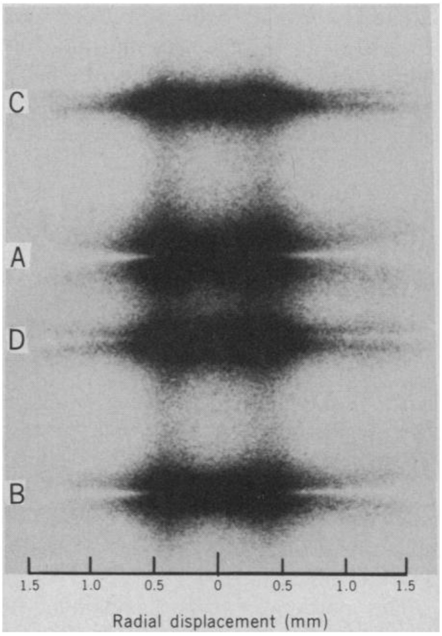

Fig. 5. Excited and ground state, ionic-absorption spectra detected at 0.100 mm from a Mg cathode sparked in Ar at 1.6 µsec after the first current. Lines are spatially resolved (± 0.02 mm) in the radial dimension relative to the vertical spark channel (0 mm displacement). Lines shown are:

A = Mg II, 2795.53 Å, $3p\ ^2P^0_{3/2} \rightarrow 3s,\ ^2S_{1/2}$

B = Mg II, 2802.70 Å, $3p\ ^2P^0_{1/2} \rightarrow 3s,\ ^2S_{1/2}$

C = Mg II, 2790.79 Å, $3d\ ^2D_{3/2} \rightarrow 3p,\ ^2P^0_{1/2}$

D = Mg II, 2798.00 Å, $3d\ ^2D_{5/2} \rightarrow 3p,\ ^2P^0_{3/2}$

petitive discharges. They did this by photographing the refraction of light produced by a nitrogen laser (*43*) as it passed through the electrode space (schlieren effect) with an apparatus fabricated by Hosch and Walters (*44*). The photographs are time-resolved (about 0.1 μsec) by the pulsed nature of the laser. Light emission from the spark is blocked by an interference filter that passes mainly the 3371-Å laser light. The laser is electronically fired before, during, or after one selected spark in a repetitive train; this procedure makes possible stroboscopic display of the discharge environments before, during, and after the spark. I report on only the last here.

The most pronounced postdischarge feature detected in refracted light is a toroidally shaped structure that surrounds the location previously occupied by the spark channel. It is observed in still or flowing Ar, N_2, or air, for Al, Cu, or Mg electrodes, when high-current (> 50 peak amperes) sparks occur. It was not detected in our first experiments with low-current, short-duration sparks in He. The structure forms out of the spark channel, spatially unfolding in time much like the mushroom cloud in a nuclear detonation (*45*). Figure 6A shows one time-resolved schlieren picture of a fully developed toroidal structure. Of particular interest is the effect this toroidal structure has on the optical aspects of spark discharge when one discharge is timed to form inside the products left from a predecessor (Fig. 6, B and C).

If one spark occurs inside the postdischarge toroid of only one predecessor (Fig. 6B), the refracted picture shows an interaction between its shock front and the toroid. The shock velocity is increased in passing through the postdischarge structure, suggesting that this region is hotter than the surrounding atmosphere. Light emitted from the inner discharge also would have to pass through the structure. Our first spectroscopic investigations with Mg cathodes indicate that strong ionic absorption occurs (*35*).

If another spark occurs coaxially inside the postdischarge structures of two predecessors (Fig. 6C), light emitted outward from the inner discharge is very weak, with a decided axial spatial structure (as in trace C, Fig. 3). Ionic absorption is very strong, with a decided off-axis radial spatial structure (as in Fig. 5). The postdischarge toroids are detected in refraction to form a layered structure. Mixing does not appear to occur. Delivery of fresh Ar coaxially to the past spark channel position sweeps away the overall structure, with some obvious mixing occurring at longer times (~1000 to 3000 μsec).

We are presently investigating the nature of the toroidal structure, and the physical mechanisms by which it forms in our experimental arrangement. Birks (*46*) has suggested that it arises from rapid (possibly radiative) cooling of the hot vapor circulating up from the cathode along the periphery of the spark channel. Were this the case, it would agree with the emission data shown in Figs. 4 and 5.

Coleman and I (*34*) interpreted our first Mg absorption data in the context that the toroid (and other parts of the postdischarge environment) contained large, but unknown, amounts of +1 ions of the electrode vapor. If this is confirmed in continuing experiments, I believe that we must also consider that precursor species to these ions could be coaxially confined around the spark channel at earlier times (while current is being conducted) by combined thermal and magnetic shaping of the moving electrode vapor ions.

In light of Klueppel's recent experiments where the absorption data on Mg were radially resolved relative to the spark channel (Fig. 5), it appears possible that +1 ions in the postdischarge environment could be formed chemically from neutral atoms as electrode vapor moved through the spark channel boundary. This possibility could well explain the coaxial confinement of neutral atom radiation.

Sense of Direction

On the basis of our earlier work and that of others (*47*), I picture the spark channel as a vertical column of coaxial cylinders with the innermost cylinder containing the most highly charged ions of the plasma gas (for example, Ar^{2+}). Moving out from the center, the cylinder would contain ions of lesser charge (such as Ar^{+}), until the ionic boundary is reached. The various cylinders could assume such an identifiable structure as a result of electron-ion recombination processes. In view of the pressures involved, I suspect that these recombinations also would occur into upper-energy (excited) daughter states (*48*). Goldstein's time-resolved, radially resolved emission data (*24*) are suggestive of such processes for Ar.

Of concern here are not the spectroscopic details of such recombinations but rather what their final expected consequences would be for plasma gases such as Ar that are known (*21*) to have metastable, excited energy levels in their neutral atom forms. In this case, recombination of the +1 ion with an electron into the upper states of the product atom will (by subsequent optical cascades) leave some of the product atoms in metastable, energetically excited atomic states (*49*). By occurring in the outer radial regions of the spark channel, the effect would cause the spark channel to be cylindrically wrapped with a long-lived,

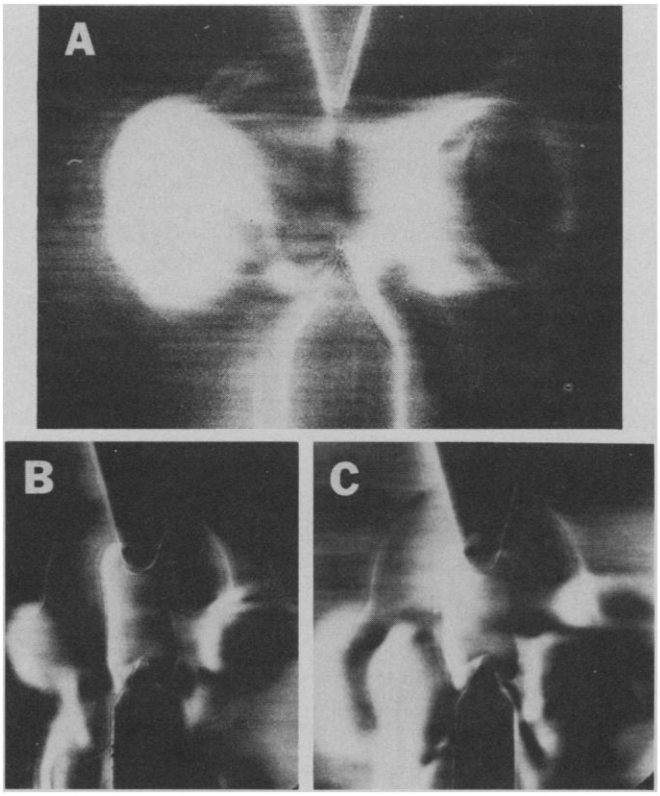

Fig. 6. Time-resolved schlieren photographs of spark discharge in Ar. The upper electrode is a W pin anode; the lower electrode is a Cu disk cathode; electrode separation, 2.0 mm; Ar flow rate, 0.5 liter/min. (A) Photograph made 150 μsec after the first current in a pulsating unidirectional discharge (150 peak amperes, 50 μsec); spark train repetition rate, 60 hertz. (B) Photograph made 5.5 μsec after the first current in the second spark in a burst of five sparks occurring once every 8.33 msec (1197.5 μsec after the first spark in the burst). (C) Photograph made 5.3 μsec after the onset of current in the fourth spark in a burst of five sparks (2746.3 μsec after the first spark).

energy-rich gas sheath. This sheath would be chemically reactive toward other species moving through it, including the cathode vapor.

The types and number of chemical reactions that could occur in such a sheath also can be estimated if one applies the criterion of energy balance between products and reactants. The total energy transferred in a postulated reaction should be conserved, with only a small portion being balanced out as a result of absorption (sink) or release (source) as kinetic energy in the reactants or products (*50*). We have used this guideline to identify by computation the excited states that the reaction products must assume in order for balance to occur within 0.5 ev. First considered were excited ions of both the plasma gas and the moving electrode vapor. For Ar^+ as the plasma ion and Cu, Ag, or Au as the vapor species, we were not able to predict what chemical reactions were occurring.

However, when the cathode material was Mg and only metastable (neutral) Ar was investigated as the other reactant, a clearer picture emerged. Only two types of reactions appeared likely, depending upon the charge of the Mg reactant.

If neutral Mg atoms enter the metastable Ar sheath, only six excited states will react with an energy balance of 0.5 ev or less (over 26,000 possibilities were computer-tested). Of these, four form a reaction product in only one excited state, and the other two give products in only three excited states. The reaction is an example of the ionization of one atom by the transfer of the excitation energy of another atom to it in a collision. This is called Penning ionization (*51*):

$$\mathrm{Mg^0\ (mixed)} + \mathrm{Ar^0}\ (^3P_0,\ ^3P_2) \rightarrow \mathrm{Mg^+\ (mixed)} + \mathrm{Ar^0}\ (^1S_0) + e^-$$

The distribution of the mixed, excited states of the Mg^0 reactant and of the Mg^+ product (*52*) is given in Table 1.

An additional reaction is expected between Mg ions and metastable Ar. It is an example of sensitized fluorescence (*53*):

$$\mathrm{Mg^+}\ (^2S_{1/2}) + \mathrm{Ar^0}\ (^3P_0,\ ^3P_2) \rightarrow \mathrm{Mg^+\ (mixed)} + \mathrm{Ar^0}\ (^1S_0)$$

The mixed excited states of the Mg^+ product are also listed in Table 1. Reactions from Mg^+ to Mg^{2+} are currently being examined.

Of interest are the spectra that are expected when the reaction products are formed. The lines expected in either emission or absorption are listed in Table 2. The spectra are relatively simple and are similar to those we have already detected and positively identified (*54*). In particular, the radial structure of the group of Mg^+ lines from 2795 to 2802 Å (for example, Fig. 5) is providing the impetus for continued spectroscopic line analysis, even to the point of measurement of absolute line intensities.

If, upon further analysis, it appears that the Mg spectra arise from excited states that are populated by collision with metastable Ar, it then remains to devise independent diagnostic tests to locate the precise spatial and temporal distribution of this reactant species. We are now adapting some of our instruments to this task. Use of a dye laser as a combined absorption probe and device to alter excited state populations (bleaching) is one part of the experiment; we intend to make observations in temporally and spatially resolved emitted, absorbed, and refracted light (*55*). The combination of the Mg^+, excited-state line reversals and the clear energy balances between metastable Ar and only a few excited Mg^0 reactants prompts the exploration.

Table 1. Predicted product and reactant states and energies for ionization or excitation, or both, of Mg by metastable ($^3P_0$ or $^3P_2$) Ar; $^3P_0$ energy = 94553.7 cm^{-1}; $^3P_2$ energy = 93143.8 cm^{-1}; both levels reverted to the $^1S_0$ ground state at 0.0 cm^{-1}.

Reactant state	Reactant energy* (cm^{-1})	Product state	Product energy (cm^{-1})	Energy defect† (ev)
		Reaction 1		
Mg^0, 3*s*, $^1S_0$	0.0	Mg^+, 3*p*, $^2P^0_{1/2,3/2}$	35,761 to 35,769	−0.35
		Reaction 2		
Mg^0, 3*p*, $^1P^0_1$	35,051	Mg^+, 4*s*, $^2S_{1/2}$	69,805	− .41
		Mg^+, 3*d*, $^2D_{5/2,3/2}$	71,490 to 71,491	− .44
		Reaction 3		
Mg^0, 4*s*, $^3S_1$	41,197	Mg^+, 4*s*, $^2S_{1/2}$	69,805	+ .36
		Mg^+, 3*d*, $^2D_{5/2,3/2}$	71,490 to 71,491	+ .15
		Reaction 4		
Mg^0, 4*p*, $^1P^0_1$	49,347	Mg^+, 4*p*, $^2P^0_{1/2,3/2}$	80,620 to 80,650	+ .02
Mg^0, 3*d*, $^1D_2$	46,403			− .17
Mg^0, 4*p*, $^3P^0_{0,1,2}$	47,841 to 47,851			−.01 to −.16
Mg^0, 3*d*, $^3D_{1,2,3}$	47,957			+.07 to −.15
		Reaction 5		
Mg^+, 3*s*, $^2S_{1/2}$	0.0	Mg^+, 5*s*, $^2S_{1/2}$	92,791	+ .04
		Mg^+, 5*p*, $^2P^0_{1/2,3/2}$	97,455 to 97,469	− .36
		Mg^+, 4*d*, $^2D_{5/2,3/2}$	93,311	− .02
		Mg^+, 4*f*, $^2F^0_{5/2,7/2}$	93,800	− .08

*Reactant and product energies used here were compiled by Goldstein (*24*) in 1969 from available literature sources to eight significant figures. Bashkin and Stoner (*52*) reported new values differing by ± 0.1 cm^{-1} from Goldstein. Only five significant figures are shown here to acknowledge this difference. †We converted from reciprocal centimeters to electron volts by using the conversion factor 8068.32 cm^{-1}/ev. The ionization potential of neutral magnesium used was 61,671.0 cm^{-1}. All calculations were done in reciprocal centimeters prior to conversion to electron volts. If both $^3P_0$ and $^3P_2$ reactions occur, only the lowest energy defect is reported. A minus sign indicates that the reactions supply less total energy than the products consume (endothermicity).

Recent work by others (*56*) indicates that ground state Ar^+ also may populate selected Mg^+ states by charge exchange. This reaction could provide another current-dependent route for level inversions in the Mg II term system.

Future Work

The picture of energy transfer presented here has several practical aspects that also give direction to our alloy analysis. Some new experiments that we contemplate require little more than stabilization of the discharges in a train. Others suggest entirely new approaches for generating the analytical signal.

One of the most straightforward experimental procedures involves taking advantage of the spatial separation between emission in low-energy, neutral-atom spectral lines and that usually classed as noise. Examples of noise emission are continuous background (Fig. 3, trace A) and lines from current-responsive species in the spark channel, for example, Ar^+ (trace B). For a positionally stable discharge, blocking the passage of noise emission to an analyzing spectrometer is done simply with an opaque mask and a focusing lens external to the instrument. The mask is sized to pass mainly radial (wing) emission from low-energy lines (trace H) from the discharge to the spectrometer. If all emission passing the mask then is spatially and temporally integrated in the spectrometer, the resulting detected spectrum is simpler (contains fewer lines) and shows higher sensitivity (higher signal-to-noise ratios).

The first masking experiments by Eaton (*57*), using photographic detection in the analysis of Al alloys, were encouraging. Sensitivity improvements of three to ten times were obtained for Pb and Cu impurities. Presently, experiments with photoelectric detection are being undertaken. This approach has the advantage that no electronic or optical modifications to the spectrometer are required. In addition to improved sensitivity, I anticipate less matrix dependency to the analytical signal (*5*), and so fewer standard samples will be needed.

The advantage of exactly stabilizing a discharge train suggests an additional analytical experiment. Most metal alloys are locally heterogeneous on their surface. A wandering spark train provides some averaging of such heterogeneity, particularly if the emission is spatially and temporally integrated. A stable train makes it possible for the heterogeneity to be monitored, such that statistical mapping of the metallurgy of the alloy surface is feasible. Rentner *et al.* showed in exploratory experiments on pure Cu (*15*) that the long-term precision of the emission from a stable spark train is high enough to warrant additional research on statistical mapping. The results may lead to new uses for spark discharge in production (quality control) applications.

I interpret the chemical aspects of spark discharge as indicating an environment of high density but relatively low kinetic temperature. Light emission occurs as a by-product of the first ionization into excited states followed by optical cascades and electron-ion recombinations to relaxed products. Emission is altered by further chemical reionization and absorption at the channel boundary and in the postdischarge environment. The processes balance to form a net emission signal, which is integrated during analysis.

The consequences of such a chemical balancing for practical analysis could be large. On the basis of energy conservation alone, I expect the channel and boundary reactions to be different for each element in a multielement alloy. Prediction of such differences by digital simulation will simplify the task of preparing matrices to accent a few lines in the spectrum of a particular element. This experiment is under way. At the same time Scheeline has begun laboratory work to cause two dissimilar metal plasmas to mix in the postdischarge environment, the intent being to restrict the resulting emission or absorption to a few known product states.

The dominance of Penning-type mechanisms at the channel boundaries and in the postdischarge environment causes, for most alloying elements, product states that strongly emit or absorb in the vacuum ultraviolet to be populated. If absorption dominates, then electrode vapor, in moving out of the spark channel and recombining into a state that can react with metastable Ar, will chemically reionize to form a vacuum-ultraviolet absorbing sheath around the channel. Thus, it may be possible to view spark discharge as a light source that absorbs in the vacuum ultraviolet (rather than as one that emits in the ultraviolet). Moreover, much of the emission we now observe may be the leakage radiation from an unexploited, signal-rich reservoir of chemical absorbers.

To explore this possibility, we have refined our computer control of the time between discharges enough to cause one to occur inside the postdischarge products of one or more predecessors (Fig. 6, B and C). The resulting structure should absorb strongly in the vacuum ultraviolet. The instruments to ascertain this, for the practical goal of deriving a strong analytical signal in a few absorption lines without attendant emission, are ready.

Klueppel is now exploring for possible population inversions in the postdischarge environment. One goal is to determine if they exist, and, if so, how electrode vapor populations can be experimentally adjusted by stimulated emission to advantage in a spectrochemical analysis. As in our earlier experiments, our goal is more signal in fewer lines (*58*).

Table 2. Expected spectra resulting from the Mg^+ excited-state population produced by the reactions predicted in Table 1.

Mg^+ excited states	Reaction number in Table 1	Wavelengths* (Å) expected in product spectrum in			
		Emission		Absorption	
$3p$, $^2P^0{}_{1/2,3/2}$	1	2,795.53		1,248.51	1,476.00
		2,802.70		1,249.93	1,478.00
				1,271.24	1,480.88
				1,273.42	1,482.89
				1,306.71	1,734.85
				1,307.88	1,737.63
				1,308.28	1,750.66
				1,309.44	1,753.47
				1,365.54	2,790.78
				1,367.26	2,798.00
				1,367.71	2,928.63
				1,369.42	2,936.51
$4s$, $^2S_{1/2}$ $3d$, $^2D_{5/2,3/2}$	2, 3	2,790.78		2,329.58	3,848.21
		2,795.53†		2,449.59	3,850.39
		2,798.00		2,660.76	4,481.13
		2,802.70†		2,660.82	4,481.33
		2,928.63		3,104.72	9,218.25
		2,936.51		3,104.81	9,244.27
				3,613.78	10,914.23
				3,615.58	10,951.78
$4p$, $^2P^0{}_{1/2,3/2}$	4	1,239.93	10,914.23	2,965.19	3,538.81
		1,240.39	10,951.78	2,967.87	3,549.52
		2,790.78†		2,968.02	3,553.37
		2,795.53†		2,969.15	4,384.64
		2,798.00†		2,971.84	4,390.54
		2,802.70†		3,165.88	4,427.99
		2,926.63†		3,168.94	4,433.99
		2,936.51†		3,172.71	8,213.99
		9,218.25		3,175.78	8,324.64
		9,244.27		3,534.97	
$3s$, $^2S_{1/2}$	5	1,025.97	3,613.78	4,013.80	6,545.97
		1,026.11	3,615.58	4,093.90	8,115.22
		1,239.93†	3,848.21	4,193.48	8,120.43
		1,240.39†	3,850.39	4,534.29	9,631.89
		1,734.85	4,481.13	4,630.88	9,632.44
		1,737.63	4,481.33	4,631.41	10,092.16
		1,750.66	8,213.99	4,739.59	10,391.76
		1,753.47	8,234.64	4,739.71	10,392.23
		2,790.78†	9,218.25†	5,401.54	21,368.91
		2,795.53†	9,244.27†	5,434.04	21,432.11
		2,798.00†	10,914.23†	5,923.37	
		2,802.70†	10,951.78†	5,928.23	
		2,928.63†	21,368.91	5,938.63	
		2,936.51†	21,432.11	5,943.50	

*Wavelengths are taken from (*52*). Lines appearing in both emission and absorption predict reversal situations as in Fig. 5. †Expected by optical cascading. Such lines would have radial intensity maxima displaced from those produced by direct state population or delayed time dependence on the discharge current peak.

References and Notes

1. D. M. Coleman and J. P. Walters, *Spectrochim. Acta Part B*, in press.
2. J. P. Walters, *Anal. Chem.* **40**, 1672 (1968).
3. L. R. Pitwell, *Appl. Spectrosc.* **16**, 77 (1962).
4. Electrode attack is considered to be of consequence if the spark causes enough vaporization of the electrode material to produce its spectrum in the gap. I have reviewed the historical aspects of cathode erosion (*6*). Quantitative measurement of the amount of cathode erosion has been reported by T. Takahashi and K. Yoshino [*Trans. Natl. Res. Inst. Metals* **10**, 53 (1968)] and shown to be proportional to the number of coulombs passed to the electrode. In our sources, the current usually is unidirectional such that only the cathode spectrum is produced [see, however, (*2*) for studies in which oscillatory current was used].
5. An example in which the spectral background intensity in a time- and space-integrated analysis of stainless steels was determined to be chiefly dependent on the Cr content of the alloy has been reported by W. R. Kennedy [*Appl. Spectrosc.* **19**, 74 (1965)]. This background was corrected to compensate for changes in alloy composition.
6. J. P. Walters, *Appl. Spectrosc.* **23**, 317 (1969); R. M. Barnes, *Anal. Chem.* **46**, 150R (1974); *ibid.* **48**, 106R (1976).
7. J. P. Cali [*Anal. Chem.* **48**, 814A (1976)] provided an excellent perspective on the magnitude of this challenge by illustrating that the preparation and certification of four samples of only one type of steel standard required well over 20 man-years and $500,000 to bring to fruition. The National Bureau of Standards currently certifies standard types for ingot iron, low-alloy steel, stainless steel, tool steel, and specialty steel, involving over 75 analyzed samples for ferrous materials alone.
8. The instrumentation mentioned here is only a part of a laboratory-wide system of spectroscopic instruments based on hardware that is sufficiently permanent during the execution of atomic emission or absorption experiments to permit quantitative measurement yet sufficiently flexible to allow inventive recycling of whole experimental arrangements between either contemporary groups or separate generations of graduate students. This hardware-based research approach is described in *Contemporary Topics in Analytical and Clinical Chemistry*, D. M. Hercules, G. M. Hieftje, L. R. Snyder, M. A. Evenson, Eds. (Plenum, New York, in press), vol. 2; also given are examples of rigid experiment beds that support mirrors, light sources, monochromators, and vacuum chambers on rails and riders as components that may be arranged into a variety of instruments as research needs dictate.
9. S. A. Goldstein and J. P. Walters, *Spectrochim. Acta Part B* **31**, 201 (1976); *ibid.*, p. 295.
10. R. J. Klueppel, D. M. Coleman, W. S. Eaton, S. A. Goldstein, R. D. Sacks, J. P. Walters, *ibid.*, in press.
11. J. P. Walters, *Anal. Chem.* **39**, 770 (1967).
12. ———, *Appl. Spectrosc.* **26**, 17 (1972).
13. A. Scheeline, D. M. Coleman, R. J. Klueppel, J. P. Walters, in preparation; D. M. Coleman and J. P. Walters, *Spectrochim. Acta Part B* **31**, 547 (1976).
14. J. P. Walters and T. V. Bruhns, *Anal. Chem.* **41**, 1990 (1969).
15. J. R. Rentner, T. Uchida, J. P. Walters, *Spectrochim. Acta Part B* **32**, 125 (1977).
16. J. P. Walters and H. V. Malmstadt, *Anal. Chem.* **37**, 1484 (1965).
17. J. P. Walters, U.S. patent 3,749,975 (31 July 1973).
18. D. P. C. Thackeray, *Nature (London)* **180**, 913 (1957).
19. J. P. Walters and S. A. Goldstein, *Sampling, Standards and Homogeneity* (Publ. ASTM STP 540, American Society for Testing and Materials, Philadelphia, 1973), pp. 45–71; see also H. Van Der Piepen and W. W. Schroeder [*J. Phys. D* **5**, 2190 (1972)] and H. Van Der Piepen [*Spectrochim. Acta Part B* **30**, 179 (1975)] for work carried out with a similar electrode arrangement. A discussion of the electrode as an integral part of one of our spark sources is in J. P. Walters and T. V. Bruhns [U.S. patent 3,653,766 (4 April 1972)] and J. P. Walters, S. A. Goldstein, and W. S. Eaton [U.S. patent 3,815,955 (11 June 1974)]. The device is commonly used in heliarc (inert gas) welding apparatus.
20. J. P. Walters, *Appl. Spectrosc.* **26**, 323 (1972).
21. The $^3P_0$ and $^3P_2$ states of Ar were determined to be metastable by photographic absorption in the 7948- and 7635-Å lines terminating on them [J. M. Anderson, *Can. J. Res.* **3**, 312 (1931)]. A. V. Phelps and J. P. Molnar [*Phys. Rev.* **89**, 1202 (1953)] reported these two levels as metastable for the emission of light by relaxation of the $^1S_0$ ground state. They indicated that the states are destroyed mainly by collisions. Atoms excited to these states thus remain so excited for times that are dependent on the pressure in the apparatus in which they are contained.
22. Thackeray (*18*) suggested that stabilization of the spark column would occur by controlled delivery of Ar to the gap. We learned by experiment that the spark current must be strictly unidirectional if the entire discharge (including particularly the cathode spot) is to be stabilized. This necessitates careful construction of the spark source, essentially from first principles, to remove coupling between inductive (or capacitive) parts of the wiring that could cause high-frequency current transients in the spark gap.
23. R. D. Sacks and J. P. Walters [*Anal. Chem.* **42**, 61 (1970)] were the first to illustrate this regularity.
24. S. A. Goldstein, thesis, University of Wisconsin (1973).
25. The term "radial" is defined differently by various investigators. Here, the convention of Sacks and Walters (*23*) and Goldstein (*24*) is used. "Radial" thus refers both to the true species distribution along a radius outward from the central (vertical) spark axis and to the projection of that distribution in two-dimensional laboratory coordinates. Scheeline and Walters (*32*) appropriately distinguished between these two interpretations by using "radial" to describe actual species distributions and "lateral" to describe their laboratory-detected absorption or emission signals. In Fig. 3, only half of the line was measured in the radial direction, with the other half entered for a symmetrical lateral presentation.
26. J. P. Walters, *Anal. Chem.* **40**, 1540 (1968).
27. S. A. Goldstein (*24*) extended my observations [(*11*), figure 15] that the axial velocity of positively charged electrode vapor ions can be described by a Boltzmann distribution. The fraction of molecules N out of a total of N_0 molecules having a velocity between V and $V + dV$ is given by

$$\frac{1}{N_0}\frac{dN}{dV} = \left[4\pi\left(\frac{m}{2\pi kT}\right)^{3/2}\right]V^2\exp\left(-\frac{mV^2}{2kT}\right)$$

with m set equal to the gram-atomic mass of the electrode material and T set equal to its boiling or sublimation temperature, and k is the Boltzmann constant. The observation is in agreement with earlier work [for example, V. E. Il'in and S. V. Lebedev, *Sov. Phys. Tech. Phys.* **7**, 177 (1963) and V. M. Zimin, *Fiz. Sb. L'vov. Gos. Univ.* **4**, 161 (1958), as described in *Spectrochemical Abstracts* **8**, (No. 3190), 81 (1958–1961)].
28. J. J. Janssen and J. D. Craggs [*J. Phys. B* **5**, 89 (1972)] have summarized the recombination processes that could be active. A review of the processes that may be most active has been given by N. H. Olsen and W. S. Huxford [*Phys. Rev.* **87**, 922 (1952)] and R. G. Fowler, W. R. Atkinson, and L. W. Marks (*ibid.*, p. 966). We suggest a three-body process largely on the basis of our spectral observations [see also Ya. B. Zel'dovich and Yu. P. Raizer, *Physics of Shock Waves and High Temperature Hydrodynamic Phenomena* (Academic Press, New York, 1966), p. 406] and not from first-principle calculations. The assignment of dominant processes is not straightforward in a plasma as impure as a multiply ionized, Ar spark channel mixed with unknown amounts of ionized metal vapors. It is expected that the recombination rates of a three-body process will be influenced by the imprisonment of vacuum-ultraviolet radiation (increasing the gas temperature and residual ionization). Such imprisonment has been reported [L. Michel and H. Fischer, *Appl. Opt.* **11**, 899 (1972)] for sparks with Ar densities reasonably comparable to ours.
29. For a comprehensive overview of such charge-transfer collisions, see J. B. Hasted, *Physics of Atomic Collisions* (American Elsevier, ed. 2, New York, 1972), pp. 612–658, and references therein.
30. W. L. Shackleford and S. S. Penner [*J. Chem. Phys.* **45**, 1816 (1966)] provide good experimental background.
31. D. M. Coleman and J. P. Walters, unpublished data.
32. A. Scheeline and J. P. Walters, *Anal. Chem.* **48**, 1519 (1976).
33. Example data are in figure 20 of the article by Rentner *et al.* (*15*). The spatial distribution of this absorption is now being measured.
34. D. M. Coleman and J. P. Walters, *J. Appl. Phys.*, **48**, 3297 (1977). See also D. M. Coleman, thesis, University of Wisconsin (1976).
35. R. J. Klueppel and J. P. Walters, in preparation.
36. Spectral line reversals in ion spectra have been observed elsewhere. For example, Michel and Fischer (*28*) reported full reversal on the Ar^{2+} lines at 1670 and 2178 Å at a discharge pressure of 8 atmospheres. A. Bardocz and F. Varsanyi [*Z. Naturforsch. Teil A* **10**, 1031 (1955)] presented photographs of ground state Mg^+ reversals.
37. Useful sources for the basics of such equilibrium calculations are the following: H. R. Griem, *Plasma Spectroscopy* (McGraw-Hill, New York, 1964), chap. 13, for the principles and formulas used in temperature measurements of plasmas; A. B. Cambel, *Plasma Physics and Magnetofluidmechanics* (McGraw-Hill, New York, 1963), chap. 6, for a quantitative introduction to the thermodynamic calculations; W. J. Pearce, in *Optical Spectrometric Measurement of High Temperatures*, P. J. Dickerman, Ed. (Univ. of Chicago Press, Chicago, 1961), pp. 125–169, for a lucid and highly readable example of the application of the theory to the temperature measurement of an arc plasma jet.
38. The instrument used to photograph the spectrum has been extensively calibrated [see, for example (*9*)] to ensure that high-fidelity image transfer occurs between points 0.03 to 0.05 mm apart in the light source and equivalent-sized regions on the detecting photographic plate. Phenomena such as astigmatism, coma, and light scattering in the emulsion [C. E. K. Mees, *The Theory of the Photographic Emulsion* (Macmillan, New York, 1954), pp. 1009–1010] are not responsible for the spatial structure of the lines in Fig. 5.
39. A. Scheeline and I have simulated the extreme case where absorbers and emitters are exactly adjacent in space. In this case, the predicted laboratory emission spatial profile may be radically distorted from a dumbbell to an axial shape if one simply increases the number of both emitters and absorbers without altering their spatial distributions. This unusual result indicates that exclusive side-on observation of spark emission is very risky if intended to depict species distributions. To avoid such risk, we intend to view the discharge from a coaxial perspective (end-on) with a spectrometer of high wavelength resolution to illustrate the absorption line spectral profile prior to the occurrence of full reversal.
40. J. W. Hosch, thesis, University of Wisconsin (1975).
41. R. J. Klueppel, D. M. Coleman, J. W. Hosch, J. P. Walters, *Spectrochim. Acta Part B*, in press.
42. J. R. Rentner and J. P. Walters, unpublished data.
43. P. Schenck and H. Metcalf, *Appl. Opt.* **12**, 183 (1973).
44. J. W. Hosch and J. P. Walters, *ibid.* **16**, 473 (1977).
45. See, for example, H. Johnston, G. Whitten, and J. Birks [*J. Geophys. Res.* **79**, 6107 (1973), and references therein].
46. J. Birks, personal communication.
47. Background information on the structure of spark channels may be found in C. Braudo and J. D. Craggs [*Int. J. Electron.* **22**, 329 (1967)] and E. A. Smårs [*Ark. Fys.* **29**, 97 (1964)].
48. C. Kenty [*Phys. Rev.* **32**, 624 (1928)] reported population of upper excited states of Ar^0 by recombination, and recent calculations [O. Wanless, *J. Phys. B* **4**, 522 (1971)] clearly take population of excited states by recombination into account from a theoretical viewpoint.
49. See, for example, O. P. Bochkova and E. Ya. Shreyder, *Spectroscopic Analysis of Gas Mixtures* (Academic Press, New York, 1965), p. 6, for tabulated radiative routes between the upper levels of Ar I and the $^3P_0$ and $^3P_2$ metastable levels.
50. A complete description of the procedure we use to diagnose reaction probability by minimizing the reaction energy defect and conservation of total reaction spin is given in Hasted (*29*), pp. 659–696.
51. O. S. Duffendack, C. L. Henshaw, M. Goyer, *Phys. Rev.* **34**, 1132 (1929); O. S. Duffendack and K. Thomson, *ibid.* **43**, 106 (1933); O. S. Duffendack and W. H. Gran, *ibid.* **51**, 804 (1937); L. D. Schearer, *Phys. Rev. A* **10**, 1380 (1974); M. G. Payne and M. H. Nayfeh, *ibid.* **13**, 595 (1976). Boumans has personally communicated to me his evidence for Penning ionization of neutral Mg to excited Mg ion by metastable Ar in a different type of electrical discharge called an inductively coupled plasma [P. W. J. M. Boumans and F. J. DeBoer, *Spectrochim. Acta Part B*, in press]. He also introduced a mathematical model to qualitatively account for the spectra observed.

52. See S. Bashkin and J. O. Stoner, Jr. [*Atomic Energy Levels and Grotrian Diagrams* (American Elsevier, New York, 1975), vol. 1, pp. 388–391] for the energy levels used in this study.
53. A. G. Mitchell and M. W. Zemansky, *Resonance Radiation and Excited Atoms* (Cambridge Univ. Press, London, 1961), pp. 59–70.
54. D. M. Coleman and R. J. Klueppel have photographed the 2795.5-Å and 2802.7-Å lines in the Mg II spectrum in full radial reversal. Klueppel has photographed the 2790.8-Å and 2798.0-Å lines in reversal (Fig. 5) as a function of the repetition rate of the spark source, and the 4481-Å lines at very high intensity. In a separate series of exploratory experiments, Coleman detected the 1734.9-, 1737.6-, 1750.7-, and 1753.5-Å lines photoelectrically. The 2428.6-Å and 2936.5-Å lines have been identified in emission but not yet in absorption. Some positive identifications have been made in the Mg I spectrum, but a full analysis is still in progress. The problem is complex as a result of the wavelength range that must be covered (~1,100 to 12,000 Å).
55. R. J. Sandeman and N. A. Ebrahim, *Appl. Opt.* **16**, 1376 (1977); M. C. E. Huber [in *Progress in Gas Dynamic Research by Optical Methods*, D. S. Dosanjh, Ed. (Plenum, New York, 1971), pp. 85–112] described the "anomalous dispersion" experiment where excited state populations are followed in refracted light. D. M. Coleman is preparing apparatus to do this at Wayne State University. With these instruments it will be possible to carry out interactive experiments with this laboratory for comparative diagnosis of the postdischarge environment with more than one spectroscopic probe [see (*8*) for details].
56. M.-U. Beth, S. Krause, W. Mayerhofer, *Z. Naturforsch. Teil A* **32**, 171 (1977).
57. W. S. Eaton, thesis, University of Wisconsin (1974).
58. Information on this type of experiment is given by W. T. Silvast, *Sci. Am.* **228**, 88 (February 1973).
59. I thank R. Riley, R. Lang, R. Schmelzer, K. Spielman, T. Weigt, and J. Peters for their assistance in the design and fabrication of our apparatus. I thank P. Brinkman and G. Beenan for their help in preparing this manuscript and J. Schrag, J. Taylor, J. Wright, and D. Evans for helpful comments. This work was supported by the National Science Foundation, the Alfred P. Sloan Foundation, and the University of Wisconsin Graduate School. I particularly thank the Fisher Scientific Company through its Jarrell-Ash Division and F. Brech for the award of a Jarrell-Ash model 750 direct-reading multielement optical spectrometer to this research effort.

H-Y Antigen and the Genetics of Sex Determination

A minimum of three genes may be required for the differentiation of the mammalian testis.

Stephen S. Wachtel

Summary. Widespread phylogenetic conservation of H-Y antigen indicates persistence of a vital function. It has been proposed that this function is the primary determination of mammalian sex. According to this proposal, the indifferent embryonic gonad is induced to differentiate as a testis in the presence of H-Y antigen, and as an ovary in the absence of H-Y antigen. But presence of H-Y antigen does not guarantee testicular differentiation. Other factors may be required: a gene that activates the H-Y structural locus, and another gene that codes for specific H-Y antigen receptors.

Female mice inoculated with cells from males of the same inbred strain produce antibody that identifies a male cell surface component called histocompatibility Y (H-Y) antigen (*1, 2*). Using this antibody in the sperm cytotoxicity test and in another serological assay, the mixed hemadsorption-hybrid antibody test, we have shown that H-Y antigen is widely conserved phylogenetically, occurring in males of all mammalian species so far tested including the human (*3*). On the basis of (i) the evolutionary persistence of H-Y structure (which signifies conservation of a vital function), (ii) the observation that the *Sxr* gene (which reverses the sex of XX mice causing them to develop as males) also specifies H-Y antigen (*4*), and (iii) the putative role of cell-surface components in the cell-cell interactions of organogenesis (*5*), we have proposed that H-Y antigen is the product of the mammalian testis-determining gene (*6*).

According to this proposal, H-Y antigen directs only the initial steps leading to differentiation of the bipotential embryonic gonad as a testis. Further male differentiation is imposed on the embryo by the action of testicular hormones, against the inherent tendency toward the female phenotype (*7*).

Because secondary male sexual differentiation is conferred by the action of testicular hormones, our hypothesis concerning the testis-determining role of H-Y antigen predicts that presence of H-Y should be correlated with presence of at least rudimentary testis regardless of karyotype or phenotypic sex. From this perspective, the genetics of primary (gonadal) sex determination is a simple matter: In the presence of the gene that confers H-Y antigenicity, the indifferent embryonic gonad becomes a testis; in the absence of this gene, the gonad develops as an ovary. But, as the following discussion will show, the genetics of primary sex determination and of H-Y antigen expression is perhaps rather more subtle.

Role of the Y Chromosome in Determination of H-Y Antigen

White blood cells from human males with two Y chromosomes (47,XYY or 48,XXYY) absorb more H-Y antibody than white blood cells from normal 46,XY males (*8*). By implication then, the amount of H-Y antigen on the surface of a cell is directly related to the number of Y chromosomes in the nucleus of that cell. This indicates that a genetic determinant of H-Y antigen expression is on the human Y chromosome, but it does not tell us whether the determinant is a structural gene that specifies the primary structure of H-Y antigen or a regulatory gene that governs the activity of a structural element. The simplest explanation is that the Y-chromosomal H-Y gene is structural, because dosage effect in this case is not easily reconciled with the existence of a Y-situated regulator. At present there is no reason to believe that the products of supernumerary regulatory genes would elicit production of "excess" H-Y antigen, given a single

---

The author is an associate at the Memorial Sloan-Kettering Cancer Center, New York 10021 and an associate professor of immunology in the Department of Pediatrics at the New York Hospital–Cornell Medical Center, New York 10021.